Semi-analytical solutions for two-dimensional elastic capsules in Stokes flow

By Michael Higley, Michael Siegel* and Michael R. Booty

Department of Mathematical Sciences and Center for Applied Mathematics and Statistics, New Jersey Institute of Technology, Newark, NJ 07102, USA

Elastic capsules occur in nature in the form of cells and vesicles and are manufactured for biomedical applications. They are widely modelled, but there are few analytical results. In this paper, complex variable techniques are used to derive semi-analytical solutions for the steady-state response and time-dependent evolution of two-dimensional elastic capsules with an inviscid interior in Stokes flow. This provides a complete picture of the steady response of initially circular capsules in linear strain and shear flows as a function of the capillary number Ca. The analysis is complemented by spectrally accurate numerical computations of the time-dependent evolution. An imposed nonlinear strain that models the far-field velocity in Taylor's four-roller mill is found to lead to cusped steady shapes at a critical capillary number Ca_c for Hookean capsules. Numerical simulation of the time-dependent evolution for $Ca > Ca_c$ shows the development of finite-time cusp singularities. The dynamics immediately prior to cusp formation are asymptotically self-similar, and the similarity exponents are predicted analytically and confirmed numerically. This is compelling evidence of finite-time singularity formation in fluid flow with elastic interfaces.

Keywords: elastic capsule; Stokes flow; complex variables

1. Introduction

An elastic capsule is a drop or bubble that is enclosed by a thin membrane and suspended in an external fluid. It serves as a simple mechanical model of a cell or vesicle that can be deformed by a fluid flow. Liquid capsules or inviscid microbubbles enclosed by a stabilizing membrane are manufactured for medical applications to enhance ultrasound images or to facilitate the delivery of drugs (Blomley *et al.* 2001). The variety of applications has motivated efforts to model and numerically simulate the behaviour of capsules in a fluid flow. Of the many numerical studies of capsules in a fluid flow, Pozrikidis (2003) gives an overview of some of the early investigations, while a recent review is provided by Barthès-Biesel (2011).

2915

This journal is © 2012 The Royal Society

Studies of capsules in fluid flow have been conducted with different membrane constitutive laws, including Hookean (Beale & Strain 2008), neo-Hookean or Skalak (Walter *et al.* 2010), and area-incompressible or inextensible membranes (Veerapaneni *et al.* 2009). Different numerical methods have also been used, such as boundary integral and immersed boundary methods. The studies have concentrated on examining the deformation of initially spherical capsules in linear strain and shear flows. The main dimensionless parameters in the problem are the capillary number Ca, which measures the relative importance of viscous and elastic tension forces, and the viscosity ratio $\lambda = \mu_i/\mu$, where μ_i and μ are the interior and exterior fluid viscosities, respectively. A particular focus is the steady response of a capsule as a function of the capillary number and the possibility of 'bursting', which is said to occur when the deformation of the membrane increases without bound in time.

An early study of three-dimensional capsule deformation in a simple shear flow (Pozrikidis 1995) conjectured the existence of a critical capillary number Ca_c above which there are no steady or equilibrium solutions. However, subsequent studies (Navot 1998; Ramanujan & Pozrikidis 1998) found steady deformation for a range of capillary number Ca and viscosity ratio λ, and instead suggested that there is no critical capillary number for bursting. The three-dimensional computations of time-dependent evolution by Lac *et al.* (2004) attain a stable steady deformation only when the capillary number lies in a range $Ca \in [Ca_L, Ca_H]$, which depends on the specific membrane constitutive law, viscosity ratio and initial membrane stress. For values of the capillary number with $Ca < Ca_L$ or $Ca > Ca_H$, compressive stresses develop in at least one of the two principal elastic tensions on the interface (see also Barthès-Biesel 1980), and when this occurs the evolution problem becomes highly unstable and the numerical method fails. Later work (Walter *et al.* 2010) using a finite-element method for the membrane obtains stable steady solutions even when compressive stresses are present. The greater stability of the finite-element method is thought to be due to numerical regularization. Three-dimensional spectral element computations (Dodson & Dimitrakopoulos 2008) for a capsule in a planar far-field strain flow show steady-state shapes with tips that change from rounded to spindled to cusped as the strain rate is increased. It was not determined analytically if there is an upper bound on the capillary number for steady states, or if true cusp singularities that are associated with a blow-up of curvature occur.

Experiments on capsules in extensional flow also reveal cusp-like shapes. The response to an imposed strain has been investigated by suspending artificial capsules in a Taylor four-roller mill. Barthès-Biesel (1991) reports stable steady states with rounded shapes at low capillary number that become cusp-like as the capillary number or strain rate is increased (Barthès-Biesel 1991, fig. 6). This is similar to cusped profiles observed by Taylor (1934) for low viscosity ratio drops or bubbles. The first numerical investigations to show development of cusp-like shapes in the evolution of strained three-dimensional capsules that are similar to the experiments of Barthès-Biesel (1991) are those of Dodson & Dimitrakopoulos (2008). The membrane in the capsule experiments eventually breaks at the tips where the curvature is greatest. In shear flow, tip break-up is sometimes observed at small viscosity ratios and at a high shear rate (Chang & Olbricht 1993).

In this paper, we derive semi-analytical solutions for the dynamics of a two-dimensional capsule in Stokes flow by generalizing a well-established complex variable technique for time-evolving bubbles in Stokes flow (Richardson 1968; Tanveer & Vasconcelos 1995; Bazant & Crowdy 2005). One motivation for this work is to provide analytical solutions to help validate the accuracy of new numerical methods for elastic membranes in flow, such as the two-dimensional studies of Veerapaneni *et al.* (2009). The only other analytical solution that we are aware of is that of Beale & Strain (2008), in which a body force drives a two-dimensional elliptical membrane with time-varying eccentricity in an otherwise quiescent flow. A second motivation is that the method we use allows a semi-analytical characterization of the steady-state response. This contrasts with three dimensions, where the steady-state response is perhaps less clear and not yet completely understood. Our method also allows us to compute time evolution when the membrane tension may become negative without introducing physical or numerical regularization. We also investigate the formation of finite-time cusp singularities, of which there are few rigorous examples in interfacial Stokes flow (e.g. Richardson 1997).

We believe that our findings are relevant to three-dimensional capsules in examples where there is a rapid growth in tip curvature and motion of the interface towards a 'pinched' cusp shape, as in Dodson & Dimitrakopoulos (2008), because, locally, the flow near a three-dimensional emerging cusp is quasi-two-dimensional. Our results, therefore, provide evidence that the local flow conditions in three dimensions are conducive to finite-time singularity formation. However, we caution that a three-dimensional capsule is capable of shapes and tip dynamics that cannot be captured by a two-dimensional model, and that elastic tension in the direction normal to the plane plays an essential role in the dynamics of a three-dimensional membrane. The relevance of a two-dimensional analytical study to a three-dimensional phenomenon has been noted in the context of drop coalescence by Eggers *et al.* (1999).

The complex variable technique is based on the construction of a conformal map $z(\zeta, t)$ from the interior of the unit disc in the ζ-plane to the viscous fluid region outside the capsule. Apart from a pole at $\zeta = 0$, the map takes the form of either a finite-order polynomial in ζ or a rational function, and the evolution is reduced to a low-order system of ordinary differential equations (ODEs) for the time-dependent map coefficients. The system of ODEs has non-local coefficients, but we find analytical expressions that determine the steady-state shape, membrane tension and solution branches of a capsule in an imposed strain or shear flow. This is complemented by spectrally accurate numerical solution of the time-dependent evolution.

The technique is limited to two-dimensional flow and an inviscid interior fluid, and for specificity we mainly consider a Hookean constitutive relation with zero bending stiffness, although we briefly consider the influence of a nonlinear constitutive relation on steady-state solutions. The results furnish a detailed picture of the steady-state response of an initially circular capsule and its time evolution in an imposed far-field flow. When the capsule is Hookean and the imposed flow is a linear shear, we find that an equilibrium shape is attained for any capillary number. In contrast, a steady shape in an imposed linear strain is attained only when the capillary number is below an analytically determined critical value Ca_c. When $Ca > Ca_c$, the deformation increases without bound and

the capsule bursts. The numerical method tracks the time-dependent evolution even when negative or compressive tensions develop, although this is usually associated with the unstable growth of round-off error. This occurs by confining the conformal map $z(\zeta, t)$ to be a finite-order polynomial or rational function, so that the generation of spurious high wavenumber modes is prevented.

We also consider an imposed nonlinear strain introduced by Antanovskii (1996) as a model for the far-field flow in Taylor's four-roller mill. Here, steady-state solutions are found to have tip curvatures that increase with capillary number, and, at a critical value Ca_{c}, the capsule exhibits zero-angled cusps. For $Ca > Ca_{c}$, there are no steady solutions and the time-dependent evolution shows the formation of finite-time cusp singularities. These cusped shapes are similar to those observed for capsules in four-roller mill experiments (Barthès-Biesel 1991) and the three-dimensional computations of Dodson & Dimitrakopoulos (2008, 2009). The dynamics in a space–time neighbourhood of a cusp singularity are shown to be self-similar, and our numerical solution tracks the similarity scaling over a 13-decade growth in the curvature, making this one of the most compelling examples of finite-time singularity formation for interfacial flow.

2. Equations of motion

Consider an elastic membrane filled with inviscid fluid and immersed in a surrounding fluid of viscosity μ. The interior and exterior fluids are assumed to have the same density, so that the capsule is neutrally buoyant and gravity is ignored. We denote the unbounded domain exterior to the capsule by Ω, and the boundary of Ω, i.e. the membrane or capsule surface, by S. The outward unit normal on S is denoted by $\hat{\mathbf{n}}$.

In the zero Reynolds number or Stokes flow limit, the dimensionless governing equations for $\mathbf{x} \in \Omega$ are

$$\nabla^{2}\mathbf{u} = \nabla p \quad \text{and} \quad \nabla \cdot \mathbf{u} = 0, \tag{2.1}$$

where $\mathbf{u}$ is the velocity of the exterior fluid and p is its pressure. The pressure of the inviscid interior fluid is constant in space and, without loss of generality, is set to zero. The area enclosed by the capsule is a conserved quantity, and lengths are non-dimensionalized by the radius R of the circular capsule of the same area. Velocities are non-dimensionalized by JR, where J is a parameter that characterizes the strain rate of the imposed flow and will be specified later. Time is non-dimensionalized by $1/J$, and pressure by $J\mu$. At $t = 0$, the capsule can have arbitrary shape and membrane tension, although we consider initial conditions for which the capsule is circular and the membrane tension is constant.

The motion of the membrane S is subject to the condition of continuity of velocity that

$$\frac{\mathrm{d}\mathbf{x}_{\mathrm{m}}}{\mathrm{d}t} = \mathbf{u}, \tag{2.2}$$

where $\mathbf{x}_{\mathrm{m}}(t) \in S$ is the location of the material point on the membrane that is initially at $\mathbf{x}_{\mathrm{m}}(0)$ and $\mathbf{u}$ is evaluated as $\mathbf{x} \to \mathbf{x}_{\mathrm{m}}$. The projection of (2.2) normal to S is the kinematic condition and determines the evolution of the capsule shape, while the projection tangential to S governs its stretching.

The dynamic boundary condition or stress balance at the capsule surface S is expressed succinctly in terms of an arc length variable s and interfacial parameterization $\mathbf{x}(s,t)$ as

$$-p\hat{\mathbf{n}} + 2\hat{\mathbf{n}} \cdot \mathbf{S} = -\frac{2}{Ca}(\tau(s,t)\mathbf{x}_s)_s, \qquad (2.3)$$

where $\tau(s,t)$ is the dimensionless membrane tension and $\mathbf{S}$ is the rate of strain tensor, with components $S_{ij} = \frac{1}{2}(\partial_{x_j} u_i + \partial_{x_i} u_j)$. Here, the effects of bending stiffness and inertia or mass of the membrane are neglected, and we have introduced the capillary number

$$Ca = \frac{2\mu JR}{E}, \qquad (2.4)$$

where E is the modulus of elasticity. Although much of the upcoming analysis is readily adaptable to other constitutive laws, for the sake of simplicity we mostly consider a membrane with a Hookean or linear elastic response, for which the tension is given by

$$\tilde{\tau} = E(\lambda - 1), \quad \lambda = \frac{\partial s}{\partial s_R}, \qquad (2.5)$$

where a tilde denotes the corresponding dimensional quantity (Pozrikidis 1992). Here λ is the stretch ratio between arc length s of the membrane at time t, and arc length s_R in a reference configuration in which there is no tension in the membrane. The area enclosed by the membrane in this reference configuration is in general different from its initial value. The tension is scaled by E, so that in dimensionless form

$$\tau = \lambda - 1. \qquad (2.6)$$

The capsule evolves in an imposed far-field flow, and we consider two examples. One is a linear flow, which is given in dimensional terms by

$$\tilde{\mathbf{u}}_\infty = \begin{pmatrix} G & B - \dfrac{\omega_\infty}{2} \\ B + \dfrac{\omega_\infty}{2} & -G \end{pmatrix} \cdot \tilde{\mathbf{x}}, \qquad (2.7)$$

where B and G characterize the strain rate, and ω_∞ is the magnitude of the vorticity of the imposed flow. Two specific examples of a linear far-field flow that we use here are a pure strain and a simple shear. A pure strain is given by $B = \omega_\infty = 0$ with non-dimensionalization $J = G$, and a simple shear is given by $G = 0$ and $B = -\omega_\infty/2$ with non-dimensionalization $J = -B$, so that the dimensionless far-field strain and shear velocity are

$$\mathbf{u}_\infty = (x, -y) \quad \text{and} \quad \mathbf{u}_\infty = (-2y, 0), \qquad (2.8)$$

respectively.

We also consider a nonlinear far-field strain as used by Antanovskii (1996), which has the dimensionless form

$$\mathbf{u}_\infty = (x + \epsilon[x^3 + 3xy^2], -y - \epsilon[3x^2 y + y^3]), \qquad (2.9)$$

where $\epsilon = G_1 R^2/G$ and G_1 is related to the geometry of the mill. Here, we set $J = G$ in the non-dimensionalization. The cubic terms provide a more faithful model of the flow generated by the counter-rotating cylinders in G. I. Taylor's

seminal four-roller mill experiments, and are derived by local expansion of the flow caused by the rollers about a point at the centre of the mill (Antanovskii 1996). With the internal pressure set to zero, the pressure far from the capsule evolves in time, i.e. in the linear and nonlinear far-field flow, respectively,

$$p_\infty = p_\infty(t) \quad \text{and} \quad p_\infty(\mathbf{x}, t) = p_\infty(t) + 6\epsilon(x^2 - y^2). \tag{2.10}$$

3. The conformal mapping technique

We give a brief overview of the application of complex variable techniques to the problem. This is a development of work by Tanveer & Vasconcelos (1995), Antanovskii (1996) and Siegel (1999, 2000), modified to account for the presence of an elastic interfacial membrane.

First, we cast the incompressible Stokes equations in terms of the stress-stream function

$$W(z, \bar{z}) = \phi(x, y) + \mathrm{i}\psi(x, y), \tag{3.1}$$

where $z = x + \mathrm{i}y$, the bar denotes complex conjugate and the stress function ϕ and stream function ψ satisfy the biharmonic equation $\nabla^4\phi = \nabla^4\psi = 0$. It is well known (Mikhlin 1957) that W has a Goursat representation

$$W(z, \bar{z}) = \bar{z}f(z) + g(z), \tag{3.2}$$

where the functions f and g are analytic in the fluid region Ω. Physical flow quantities can readily be expressed in terms of f and g (Langlois 1964)

$$p - \mathrm{i}\omega = 4f'(z), \tag{3.3}$$

$$u_1 + \mathrm{i}u_2 = -f(z) + z\bar{f}'(\bar{z}) + \bar{g}'(\bar{z}) \tag{3.4}$$

and

$$s_{11} + \mathrm{i}s_{12} = z\bar{f}''(\bar{z}) + \bar{g}''(\bar{z}), \tag{3.5}$$

where ω is the fluid vorticity, $\bar{f}$ denotes the (analytically continued) conjugate function $\bar{f}(z) = \overline{f(\bar{z})}$ and the prime denotes derivative. Here, $u_1 + \mathrm{i}u_2$ is the complex velocity, and $s_{11} + \mathrm{i}s_{12}$ is a complex rate-of-strain function.

Equations (3.3)–(3.5) are used to express the boundary conditions on the capsule surface in terms of $f(z)$ and $g(z)$. When substituted into the stress balance (2.3) with outward normal $n_1 + \mathrm{i}n_2 = \mathrm{i}z_s$, an integration with respect to s gives

$$f(z) + z\bar{f}'(\bar{z}) + \bar{g}'(\bar{z}) = -\mathrm{i}\frac{\tau(s, t)}{Ca}z_{\mathrm{s}} \tag{3.6}$$

on the capsule surface, where a constant of integration has been set to zero and we have emphasized the dependence of the membrane tension τ on the arc length s. An equation for the velocity on the capsule surface follows when g is eliminated between (3.4) and (3.6), namely

$$u_1 + \mathrm{i}u_2 = -\frac{\mathrm{i}\tau(s, t)}{Ca}z_{\mathrm{s}} - 2f(z). \tag{3.7}$$

We introduce a conformal map $z(\zeta, t)$ that takes the unit disc $\Gamma = \{\zeta : |\zeta| < 1\}$ in the ζ-plane onto the fluid region Ω in the z-plane. The form of the map is

$$z(\zeta, t) = \frac{\alpha(t)}{\zeta} + h(\zeta, t), \tag{3.8}$$

where $h(\zeta, t)$ is analytic and $z_\zeta(\zeta, t) \neq 0$ in $|\zeta| \leq 1$ over some time interval. Without loss of generality, we take $h(0, t) = 0$, and to follow previous work we choose $\alpha < 0$ for a linear far-field flow and $\alpha > 0$ for a nonlinear far-field flow.

4. Linear imposed flow

The form of the imposed flow as $z \to \infty$ determines the behaviour of $f(z(\zeta, t), t)$ and $(\mathrm{d}g/\mathrm{d}z)(z(\zeta, t), t)$ as $\zeta \to 0$. From (3.3) and (3.8), for any linear imposed flow

$$f(\zeta, t) \sim \frac{\alpha(t)\,(p_\infty - \mathrm{i}\omega_\infty)}{4\zeta} + C(t) + O(\zeta), \tag{4.1}$$

where $C(t)$ is a constant of integration, and $\omega_\infty = \lim_{|z| \to \infty} \omega(z, t)$ is the dimensionless vorticity at infinity, which is $\omega_\infty = 0$ for a pure strain and $\omega_\infty = 2$ for a simple shear. Similarly, from (3.4), (3.8) and (4.1)

$$\frac{\mathrm{d}g}{\mathrm{d}z}(\zeta, t) \sim \frac{\alpha(t)}{\zeta} H + \overline{C(t)} + O(\zeta) \tag{4.2}$$

as $\zeta \to 0$, where $H = (G - \mathrm{i}B)/J$, so that $H = 1$ for the imposed strain flow in (2.8) and $H = i$ for the shear flow. The dimensionless far-field pressure $p_\infty(t)$ and the function $C(t)$ are to be determined.

A formula for the map $z(\zeta, t)$ in $|\zeta| < 1$ is derived from the normal component of (2.2) followed by the application of the Poisson integral formula, with the result that (Tanveer & Vasconcelos 1995)

$$z_t + 2f = \zeta z_\zeta[I(\zeta, t) + \mathrm{i}K], \tag{4.3}$$

where

$$I(\zeta, t) = \frac{1}{2\pi\mathrm{i}} \int_{|\zeta'|=1} \frac{\mathrm{d}\zeta'}{\zeta'} \left[\frac{\zeta' + \zeta}{\zeta' - \zeta}\right] \left[\frac{\tau(\zeta', t)}{Ca|z_\zeta(\zeta', t)|}\right]. \tag{4.4}$$

Note that $I(\zeta, t)$ depends on the elastic tension at $z(\zeta, t)$ non-locally via the term $\tau(\zeta', t)$ in the integrand. The constant K is determined by expanding (4.3) as $\zeta \to 0$ and equating singular terms to find

$$K = \frac{\omega_\infty}{2} \quad \text{and} \quad p_\infty(t) = -2\left[I(0, t) + \frac{\dot{\alpha}}{\alpha}\right]. \tag{4.5}$$

Equation (4.3) is a relation between the Goursat function f and the map $z(\zeta, t)$, and another relation is yet to be found. Equations that determine the map are presented subsequently.

An equation for $g'(z(\zeta, t), t)$ is formulated when f is eliminated between (3.6) and (4.3), with the result that (Tanveer & Vasconcelos 1995)

$$
\frac{\mathrm{d}g}{\mathrm{d}z}(\zeta, t) = \frac{\bar{z}(\zeta^{-1}, t)}{2} \left\{ \frac{z_t(\zeta, t)}{z_\zeta(\zeta, t)} - \zeta I_\zeta(\zeta, t) - \left[1 + \frac{\zeta z_{\zeta\zeta}(\zeta, t)}{z_\zeta(\zeta, t)} \right] [I(\zeta, t) + iK] \right\}
$$
$$
+ \frac{\bar{z}_\zeta(\zeta^{-1}, t)}{2\zeta} [I(\zeta, t) + iK] + \frac{\bar{z}_t(\zeta^{-1}, t)}{2}, \tag{4.6}
$$

which is originally valid on $|\zeta| = 1$ but is extended off the unit circle by analytic continuation. The requirement that the right-hand side of (4.6) is analytic in $|\zeta| < 1$ except for a known pole at $\zeta = 0$ determines time evolution of the map $z(\zeta, t)$.

(a) Exact truncation

A key finding of the analysis of Tanveer & Vasconcelos (1995), which also holds here for the analogous problem with an elastic interface, is that the Laurent expansion of the conformal map (3.8) about $\zeta = 0$ exactly truncates. More precisely, the map is given by

$$
z(\zeta, t) = \alpha(t)\zeta^{-1} + \sum_{n=1}^{N} h_n(t)\zeta^n, \tag{4.7}
$$

for some finite $N \geq 1$ and $t > 0$ if it has the same form at $t = 0$. In this way, the time evolution of the surface is reduced to that of a finite-dimensional system of spatially non-local ODEs.

General evolution equations for $h_n(t)$ for a bubble in a linear imposed flow are derived in Tanveer & Vasconcelos (1995). The same equations occur here, with the exception that the interfacial tension $\tau(\zeta, t)$ depends on space and time. We consider the case $N = 1$, with an initially circular capsule so that $h_1(0) = 0$.

When h_1 is relabelled β, the evolution equations for a pure strain flow (2.8) are

$$
z = \frac{\alpha}{\zeta} + \beta\zeta \quad \text{with} \quad \alpha^2 - \beta^2 = 1, \tag{4.8}
$$

$$
\frac{\mathrm{d}}{\mathrm{d}t}(\alpha\beta) = -2\hat{I}_0\alpha\beta + 2\alpha^2 \tag{4.9}
$$

and
$$
\alpha(0) = -1, \quad \beta(0) = 0, \tag{4.10}
$$

where
$$
\hat{I}_0(t) = \frac{1}{2\pi} \int_0^{2\pi} \frac{\tau(e^{i\nu}, t)}{Ca|z_\zeta(e^{i\nu}, t)|} \, \mathrm{d}\nu. \tag{4.11}
$$

Here $\hat{I}_0(t)$ is $I(\zeta, t)$ at $\zeta = 0$, and we have parameterized the unit circle by $\zeta' = e^{i\nu}$. These equations are easily derived by equating singular terms in (4.6). We note that the capsule shape is always elliptical with a time-dependent aspect ratio. By symmetry, β is real and the major axis of the ellipse is aligned with the x-axis.

In the case of a simple shear flow,

$$\alpha^2 - |\beta|^2 = 1 \tag{4.12}$$

and

$$\frac{\mathrm{d}}{\mathrm{d}t}(\alpha\bar{\beta}) = -2(\hat{I}_0 + \mathrm{i})\alpha\bar{\beta} + 2\mathrm{i}\alpha^2, \tag{4.13}$$

with initial data (4.10). The capsule is still an ellipse for $t > 0$, but is oriented at a non-zero angle with respect to the x-axis.

(b) Membrane tension

An expression for the membrane tension $\tau(\nu, t)$ in terms of the map $z(\zeta, t)$ is required to close the system of equations (4.8)–(4.11) or (4.10)–(4.13). The result is summarized here. Although the derivation in the context of two dimensions and complex variables is new, the details are given in the electronic supplementary material, §1. A general non-material parameterization of the interface at time t is denoted by $z(\mathrm{e}^{\mathrm{i}\nu}, t)$. We define the 'backward' map $\nu_0(\nu, t)$ such that $z(\mathrm{e}^{\mathrm{i}\nu_0(\nu,t)}, 0)$ is the location at $t = 0$ of the material point that at time t is located at $z(\mathrm{e}^{\mathrm{i}\nu}, t)$. The expression for $\tau(\nu, t)$ in terms of the backward map $\nu_0(\nu, t)$ is

$$\tau(\nu, t) = \frac{|z_\zeta(\mathrm{e}^{\mathrm{i}\nu}, t)|}{|z_\zeta(\mathrm{e}^{\mathrm{i}\nu_0(\nu,t)}, 0)|\nu_0'(\nu, t)}(1 + \tau(\nu_0(\nu, 0), 0)) - 1. \tag{4.14}$$

This requires the evolution of the backward map $\nu_0(\nu, t)$, which is given by

$$\frac{\partial \nu_0}{\partial t} = \frac{\partial \nu_0}{\partial \nu}\left[H\left(\frac{\tau}{Ca|z_\zeta|}\right) + K\right], \quad \nu_0(\nu, 0) = \nu, \tag{4.15}$$

where

$$H\left(\frac{\tau}{Ca|z_\zeta|}\right) = \frac{1}{2\pi}\int_0^{2\pi}\frac{\tau(\mathrm{e}^{\mathrm{i}\theta}, t)}{Ca|z_\zeta(\mathrm{e}^{\mathrm{i}\theta}, t)|}\cot\left(\frac{\nu - \theta}{2}\right)\mathrm{d}\theta \tag{4.16}$$

is a Hilbert transform. We note that the evolution of the backward map (4.15) is independent of the choice of constitutive law, which enters the analysis only via (4.14). A useful formula for the velocity on the capsule surface is

$$u_1 + \mathrm{i}u_2 = -\mathrm{i}\zeta z_\zeta\left[H\left(\frac{\tau}{Ca|z_\zeta|}\right) + K\right] + z_t, \tag{4.17}$$

which is derived in the electronic supplementary material, §1.

(c) Steady states

Here we derive closed-form expressions for steady capsule shapes and elastic tension. First, from (2.5)

$$\frac{\partial s_R}{\partial \nu} = \frac{\partial s_R}{\partial s}\frac{\partial s}{\partial \nu} = \frac{|z_\zeta(\mathrm{e}^{\mathrm{i}\nu}, t)|}{\lambda(\nu, t)},$$

which holds in the general time-dependent case. The reference length L of the membrane is therefore given by

$$L = \int_0^{2\pi} \frac{|z_\zeta(e^{i\nu}, t)|}{\lambda(\nu, t)} \, d\nu. \tag{4.18}$$

Since L is conserved, this is also the reference length of the equivalent circular membrane at $t = 0$ with unit radius and a spatially uniform tension τ_0, so that

$$L = \frac{2\pi}{\tau_0 + 1}. \tag{4.19}$$

Conservation of total reference length therefore implies that

$$\int_0^{2\pi} \frac{|z_\zeta(e^{i\nu}, t)|}{\lambda(\nu, t)} \, d\nu = \frac{2\pi}{\tau_0 + 1}. \tag{4.20}$$

(i) *Pure strain*

The symmetry of a pure strain implies that $u_1 + iu_2 = 0$ on the surface of a steady capsule, so that with $z_t = K = 0$ equation (4.17) gives

$$\frac{1}{2\pi} \int_0^{2\pi} \frac{\tau(e^{i\theta})}{Ca|z_\zeta(e^{i\theta})|} \cot\left(\frac{\nu - \theta}{2}\right) d\theta = 0. \tag{4.21}$$

The solution of (4.21) is given by the Hilbert formula (Mikhlin 1957), namely $\tau/(Ca|z_\zeta|) = C = \text{constant}$. When this is substituted in the steady-state version of the evolution equation (4.9), use of (4.8), (4.10) and (4.11) implies $C = -\sqrt{1 + \beta^2}/\beta$, so that

$$\tau = -Ca|z_\zeta|\frac{\sqrt{1 + \beta^2}}{\beta}. \tag{4.22}$$

This is the required expression for the membrane tension, where we note that the time-dependent evolution of (4.8)–(4.11) implies that $\beta < 0$. Then, if we substitute Hooke's law $\lambda = \tau + 1$ in (4.20), eliminate τ using (4.22) and set the initial tension $\tau_0 = 1$, we have

$$\int_0^{2\pi} \frac{|z_\zeta(e^{i\nu})|}{-Ca(1 + \beta^2)^{1/2}\beta^{-1}|z_\zeta(e^{i\nu})| + 1} \, d\nu = \pi, \tag{4.23}$$

which determines the steady-state solution branch, because it gives the capillary number Ca in terms of the conformal map parameters β and $\alpha = -\sqrt{1 + \beta^2}$ per (4.8).

Equation (4.23) simplifies in the asymptotic limits of small and large $|\beta|$, and it is easily shown that $Ca \sim -\beta$ as $\beta \to 0^-$ and $Ca \to 2$ as $\beta \to -\infty$. Further analytical simplification of (4.23) for arbitrary β is not possible, and we use Newton iteration to find the capillary number Ca in terms of the map parameter β. The results are plotted in figure 1, which shows the steady-state solution branch as a solid line. This is compared with the results of numerical computation of the time-dependent problem (see §4d), which for large t approach steady-state values that are in good agreement with the steady solution branch (4.23). The capsule profiles at different points on the steady solution branch are also shown together
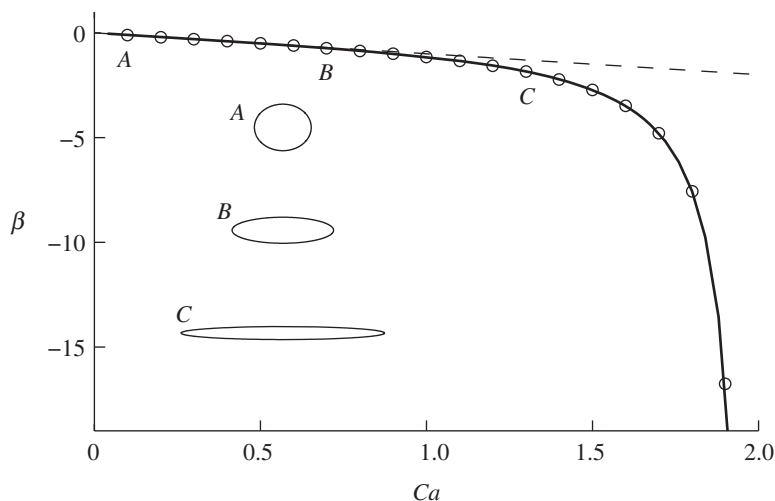
Figure 1. Steady-state values of the map parameter β for linear strain flow versus Ca with $\tau_0 = 1$ (solid line), compared with values obtained from time-dependent computation at large t (circles). An asymptotic solution for small deformation is shown by a dashed line. Representative steady profiles are given at points A, B and C.
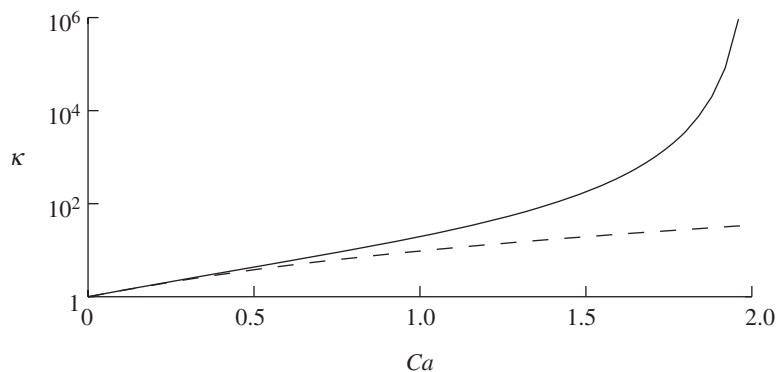

Figure 2. Curvature κ (log scale) at the tip of a steady-state capsule ($\tau_0 = 1.0$) in a linear strain (solid line) and a linear shear (dashed line) versus capillary number Ca.

with the asymptotic calculation for small $|\beta|$ (dashed line). The asymptotic behaviour $Ca \to 2$ as $\beta \to -\infty$ is clearly visible in figure 1 and indicates that there are no steady solutions for Ca greater than a critical capillary number $Ca_c = 2$. Figure 2 shows the steady-state curvature at the capsule tip versus Ca as a solid line. The tip curvature grows rapidly with Ca as $Ca \to Ca_c$, which also occurs for three-dimensional capsules in the same linear strain flow (see Dodson & Dimitrakopoulos 2009). We see below in §4d that, when $Ca > Ca_c$, the capsule 'bursts'—that is, it elongates without bound. A critical capillary number, above which only bursting can occur, is also found for a two-dimensional bubble in a pure strain (Tanveer & Vasconcelos 1995).

To check the steady solutions presented here, we have verified that the fluid stress on a solid elliptical cylinder in a pure strain as calculated by the classical theory of Jeffery (1922) is identical to that on a steady elastic capsule of the same shape when computed by our conformal map technique. Details are presented in the electronic supplementary material, §5.

(ii) *Pure strain: nonlinear constitutive law*

The existence of a critical capillary number for bursting depends on the membrane's constitutive law. In addition to the linear Hookean law, we briefly consider nonlinear constitutive laws for a membrane in uniaxial extension (Barthès-Biesel *et al.* 2002), where the tension τ has the asymptotic behaviour $\tau \sim \lambda^a$ for $\lambda \gg 1$. We find that a steady capsule shape exists for any capillary number when $a > 1$, but there is a critical capillary number for bursting when $0 < a \leq 1$. For example, we find that time-dependent computations using a Skalak strain hardening law with $a = 4$ give steady-state solutions in which the conformal map parameter β satisfies $|\beta| \propto Ca^{1/3}$ for $Ca \gg 1$ (recall that capsule deformation increases with the magnitude of β). A derivation of this scaling relation follows on noting that when $|\beta| \gg 1$ a significant portion of the membrane is highly stretched with $\lambda \gg 1$. Substitution of $\lambda \sim \tau^{1/a}$ in (4.20) and use of (4.22) then gives

$$\left(\frac{|\beta|}{Ca\sqrt{1+\beta^2}} \right)^{1/a} \int_0^{2\pi} |z_\zeta(\mathrm{e}^{\mathrm{i}\nu})|^{(a-1)/a}\,\mathrm{d}\nu = \frac{2\pi}{\tau_0 + 1}. \qquad (4.24)$$

Here, we have assumed that $\lambda \gg 1$ over the entire membrane with negligible error. The map (4.8) with $|\beta| \gg 1$ now implies that

$$Ca^{-1/a}|\beta|^{(a-1)/a} \int_0^{2\pi} |1 - \mathrm{e}^{-2\mathrm{i}\nu}|^{(a-1)/a}\,\mathrm{d}\nu = \frac{2\pi}{\tau_0 + 1}. \qquad (4.25)$$

When $a > 0$, the integral is such that $0 < c_0 < \int_0^{2\pi} |1 - \mathrm{e}^{-2\mathrm{i}\nu}|^{(a-1)/a}\,\mathrm{d}\nu < c_1$ for constant c_0 and c_1, and it follows that

$$|\beta| \sim Ca^{1/(a-1)}. \qquad (4.26)$$

This implies that, for $a > 1$, steady states exist for all Ca, and, for example, a Skalak law with $a = 4$ recovers $|\beta| \sim Ca^{1/3}$. When $0 < a < 1$, we see from (4.26) that $Ca \to 0$ as $|\beta| \to \infty$, implying that there is a maximum capillary number Ca_c for existence of a steady solution—when $Ca > Ca_c$, the capsule bursts. The degenerate case $a = 1$ corresponds to constant Ca as $|\beta| \to \infty$, consistent with the analysis of §4c(i). Numerical computations of axisymmetric capsule evolution in an imposed strain flow (Barthès-Biesel *et al.* 2002) find steady states for a wide range of capillary number in the case of a Skalak law with $a = 4$, consistent with the results here, but find a critical capillary number for bursting when using a neo-Hookean law with $a = 3/2$, which differs from our two-dimensional result.

(iii) *Simple shear*

In a simple shear flow, the capsule evolves to a steady shape, but the membrane moves tangentially in a 'tank-treading' motion. The tension τ and the tangential velocity of the membrane $v = \mathbf{u} \cdot \hat{\mathbf{t}}$ are steady, so that $\tau = \tau(s)$ and $v = v(s)$, where

s is a parameterization of the surface by arc length. Analytical expressions for these functions that determine the steady-state solution branch are derived in the electronic supplementary material, §2.

This confirms by analytical means that steady states exist for all values of the capillary number Ca. Indeed, we find that, for large values of Ca, the map parameter $|\beta| \sim 2Ca$ and the deformation $\rho \to 1$ as $Ca \to \infty$, where ρ is defined as the ratio of the difference of the semi-axes, lengths to their sum.

(d) Time evolution

Numerical solution of the initial value problem, which is (4.8)–(4.11) for a pure strain or (4.10)–(4.13) for a simple shear together with (4.14) and (4.15), is based on a uniform discretization in the ζ-plane, $\zeta_j = e^{i\nu_j}$ with $\nu_j = 2\pi(j-1)/N$ for $j = 1, \ldots, N$. The method is spectrally accurate; spatial derivatives are calculated via wavenumber multiplication of Fourier coefficients, the non-local term (4.11) is computed by the trapezoidal rule and the Hilbert transform $H(f)$ in (4.15) is computed from the Fourier coefficients $\hat{f}_k$ of f by

$$H(f) = f_+ - f_-,$$

where $f_+ = \sum_{k>0} \hat{f}_k\, e^{ik\nu}$ and $f_- = \sum_{k<0} \hat{f}_k\, e^{ik\nu}$. Thus, non-local and convolution terms are evaluated efficiently in $O(N \log N)$ operations via the fast Fourier transform alone. This is a special feature of the conformal map parameterization, and contrasts with a standard boundary integral formulation for which a fast multi-pole or related method is necessary to achieve an $O(N \log N)$ or better implementation (Kropinski 2001). Time-stepping is accomplished by the DOPRI 5(4) implementation of a Runge–Kutta–Fehlberg method (Stoer & Bulirsch 2002). In practice, the function $\nu_0(\nu, t)$ can generate a large number of Fourier modes with amplitude above round-off, and when necessary N is increased. The range of N used here is 1024 to 16 384. A spectral filter is used to prevent the spurious growth of round-off error (Krasny 1986). The spectral accuracy of the time-dependent computations is demonstrated in the electronic supplementary material, §3.

In figure 3, we show examples of time-dependent capsule deformation with an imposed far-field pure strain and simple shear flow. In both examples, the capsule deforms from its initially circular state to a steady ellipse. The capsule major axis remains aligned with the x-axis for a pure strain as the deformation increases to its steady-state value. By way of contrast, in a simple shear flow, the capsule major axis rotates to a steady limiting value, and the deformation slightly overshoots its steady value before relaxing back to it. This feature is also observed in the three-dimensional capsule computations of Lac *et al.* (2004). In the steady state, the capsule 'tank-treads'—that is, the capsule membrane rotates with non-zero tangential velocity.

Figure 4 depicts the time-dependent length of the semi-major axis l for a capsule in a pure strain with $Ca > Ca_c$. In this case, the capsule 'bursts'—that is, the deformation increases in time without bound.

Figure 5 shows the minimum membrane tension on a steady-state capsule in linear strain and shear flows for different initial tension τ_0. The plot of minimum tension versus capillary number for a capsule in a linear strain flow (figure 5*a*) shows that the minimum tension goes to zero as Ca approaches the critical

(a) (b)

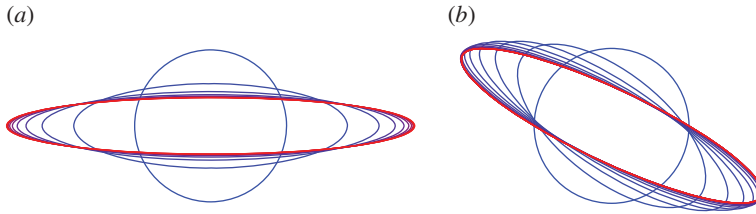Figure 3. The time evolution of a capsule in (a) a pure strain flow and (b) a simple shear flow with $Ca = 1$ and $\tau_0 = 1$. The capsule profiles are shown at intervals of (a) $\Delta t = 1.0$ and (b) $\Delta t = 0.5$. (Online version in colour.)
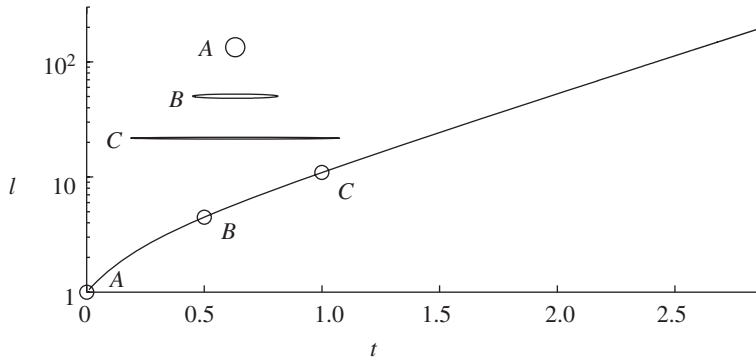

Figure 4. Length $l = |\alpha| + |\beta|$ of the semi-major axis of a capsule in a pure strain with $Ca = 5.0$ and $\tau_0 = 1$.
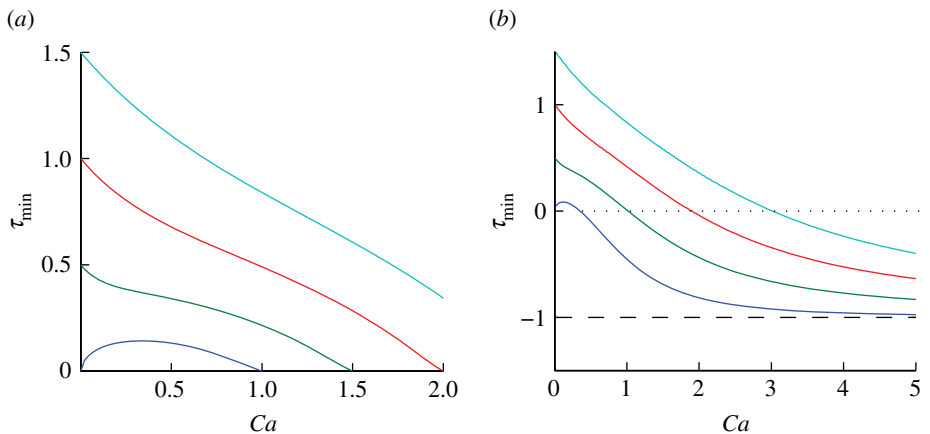
(a) (b)

Figure 5. Minimum steady-state tension τ_{min} (solid lines) versus Ca for a capsule in (a) a linear strain flow and (b) linear shear flow with initial tension $\tau_0 = 0.0, 0.5, 1.0, 1.5$ (from left to right). In a linear shear flow, the lower bound on the tension is $\tau = -1$. (Online version in colour.)

capillary number Ca_c for bursting, which can be verified by analysis of the steady-state solution branch. This minimum tension occurs at the capsule ends, and as $Ca \to Ca_c$ both the curvature and capsule length tend to infinity. For a capsule in a linear shear (figure 5*b*), we find that there is a range of sufficiently small capillary number for which the minimum tension is positive, but, at a larger capillary number, the minimum tension is negative; so the membrane is in a state of local compression.

Even if negative tension does not occur in the steady state, in our computations, we have observed that transient compression can occur during evolution towards the steady state. In this event, the initial value problem for the map $z(\zeta, t)$ in the 'physical' domain $|\zeta| \le 1$ is ill-posed. By truncating the map at finite order (4.7), we prevent the generation of new singularities in the finite part of the complex ζ-plane, that is, the only singularities of $z(\zeta, t)$ are at $\zeta = 0$ and $\zeta = \infty$. The map truncation (4.7) is exact (i.e. involves no approximation) and, in the absence of some means of either physical or numerical regularization, it makes the problem well-posed. However, it suppresses or eliminates instability that would, for example, be triggered by spontaneous noise in a physical experiment when membrane tension becomes negative.

Barthès-Biesel notes in recent papers (e.g. Barthès-Biesel 2011) that numerical regularization is present in her work and this has enabled computations to continue with negative membrane tension. Here, there is no or minimal numerical regularization, but instead regularization is provided by truncation of the map.

5. Nonlinear far-field flow

Here, we consider the nonlinear strain (2.9) that models the imposed velocity of Taylor's four-roller mill. The analysis is modified to account for the nonlinear terms in the imposed flow, and we present some of the equations without derivation, referring the reader to Antanovskii (1996) and Siegel (2000) for details.

The polynomial conformal map of (4.7) is no longer preserved by the evolution, and instead we take the map from the unit disc $|\zeta| < 1$ to the fluid domain to be a rational function of the form

$$z(\zeta, t) = \frac{\sum_{k=0}^{N} \gamma_k(t) \zeta^{2k}}{\zeta \prod_{n=1}^{N}(1 - \zeta^2 \zeta_n^{-2}(t))}, \tag{5.1}$$

which, with real coefficients, represents a shape with symmetry about the coordinate axes. For the specific far-field flow (2.9), it is shown for time-dependent deformation of a bubble in Siegel (2000) that the map exactly truncates, i.e. no higher powers of ζ are generated in the numerator or denominator during time evolution, similar to truncation of the map (4.7).

A general procedure to derive evolution equations for the map parameters $\gamma_k(t)$ and $\zeta_n(t)$ is given by Crowdy & Siegel (2005). Here, we restrict our analysis to $N = 1$, and write the map as

$$z(\zeta, t) = \frac{\alpha(t) + \beta(t)\zeta^2}{\zeta(1 - \gamma(t)\zeta^2)}, \quad \text{with} \quad \alpha(0) = 1, \beta(0) = \gamma(0) = 0, \tag{5.2}$$

which describes the evolution of an initially circular capsule. We choose $\alpha(t) > 0$ to follow previous work.

For the nonlinear imposed flow, the boundary conditions (4.1) and (4.2) generalize and are given in the electronic supplementary material, §4, while equation (4.3) for the conformal map in $|\zeta| < 1$ generalizes to become

$$z_t + 2f = \zeta z_\zeta \left[-\frac{\epsilon \alpha^2}{\zeta^2} + I(\zeta, t) \right], \tag{5.3}$$

where now

$$I(\zeta, t) = \frac{1}{2\pi i} \int_{|\zeta'|=1} \frac{d\zeta'}{\zeta'} \left[\frac{\zeta' + \zeta}{\zeta' - \zeta} \right] \left[\frac{\tau(\zeta', t)}{Ca |z_\zeta(\zeta', t)|} + \mathrm{Re}\left(\frac{\epsilon \alpha^2}{\zeta'^2} \right) \right]. \tag{5.4}$$

Elimination of $f(z)$ between (3.6) and (5.3) gives an equation for $\frac{dg}{dz}(\zeta, t)$, which is now

$$\frac{dg}{dz}(\zeta, t) = \frac{\bar{z}(\zeta^{-1}, t)}{2} \left\{ \frac{z_{\zeta t}(\zeta, t)}{z_\zeta(\zeta, t)} - \zeta I_\zeta(\zeta, t) - \frac{2\epsilon \alpha^2}{\zeta^2} - \left[1 + \frac{\zeta z_{\zeta\zeta}(\zeta, t)}{z_\zeta(\zeta, t)} \right] \right.$$
$$\left. \times \left[I(\zeta, t) - \frac{\epsilon \alpha^2}{\zeta^2} \right] \right\} + \frac{\bar{z}_\zeta(\zeta^{-1}, t)}{2\zeta} \left[I(\zeta, t) - \frac{\epsilon \alpha^2}{\zeta^2} \right] + \frac{\bar{z}_t(\zeta^{-1}, t)}{2}. \tag{5.5}$$

Evolution equations for the conformal map parameters are derived in Crowdy & Siegel (2005) and Siegel (2000) and take the form

$$\frac{d\beta}{dt} = 2\alpha \frac{\alpha - \beta I(\sqrt{\gamma}, t)}{\alpha + \beta \alpha'(\beta)}, \quad \alpha = \left[\frac{2(1 + \beta^2)}{c_1 + \sqrt{c_1^2 - c_2}} \right]^{1/2}, \quad \gamma = \epsilon \alpha \beta, \tag{5.6}$$

where

$$c_1 = 1 - \epsilon \beta^2 [2(1 - \epsilon) + \epsilon \beta^2], \quad c_2 = 4\epsilon^2 \beta^2 (1 + \beta^2)[3 + \epsilon(2 + \epsilon)\beta^2],$$

with $\alpha(0) = 1$, $\beta(0) = \gamma(0) = 0$ and $\alpha'(\beta)$ denotes a derivative with respect to β. The map (5.2) has simple poles at $\zeta = 0$ and outside the unit disc at $\zeta = \pm 1/\sqrt{\gamma}$, while the expression for $g'(z)$ of equation (5.5) is analytic for $0 < |\zeta| \leq 1$. The terms $\bar{z}_\zeta(\zeta^{-1}, t)$ and $\bar{z}_t(\zeta^{-1}, t)$ have poles of order 2 at $\zeta = \pm \sqrt{\gamma}$ inside the disc. Removal of the resulting pole of order 2 in $g'(z)$ gives the first equation in (5.6). The second equation follows either from removal of the pole of order 1 at $\zeta = \pm \sqrt{\gamma}$ or more simply by conservation of capsule area. The strength of the simple pole in $g'(z)$ at $\zeta = 0$ is equated between (5.5) and (4.2) of the electronic supplementary material to find the third equation of (5.6).

The membrane tension is still given by (4.14), while the equation for the backward map $\nu_0(\nu, t)$ is derived by contour deformation to analytically continue (5.3) onto $|\zeta| = 1$ and analogous steps from (1.2) to (1.8) of the electronic supplementary material, with the result that

$$\frac{\partial \nu_0}{\partial t} = \frac{\partial \nu_0}{\partial \nu} \left[H \left(\frac{\tau}{Ca |z_\zeta|} + \mathrm{Re}\left(\frac{\epsilon \alpha^2}{\zeta^2} \right) \right) + \epsilon \alpha^2 \mathrm{Im}(\zeta^2) \right], \quad \nu_0(\nu, 0) = \nu \tag{5.7}$$

on $|\zeta| = 1$.

(a) Steady states

We eliminate $f(z)$ between (3.7) and equation (4.5) of the electronic supplementary material and note that in the steady state $z_t = 0$ and $u_1 + iu_2 = 0$ on the capsule surface, so that

$$H\left(\frac{\tau}{Ca|z_\zeta|} + \mathrm{Re}\left(\frac{\epsilon\alpha^2}{\zeta^2}\right)\right) + \epsilon\alpha^2\sin 2\nu = 0. \qquad (5.8)$$

This can also be found from (5.7) by noting that in the steady state $\partial_t\nu_0 = 0$. By the Hilbert formula (Mikhlin 1957), this has general solution

$$\frac{\tau(\mathrm{e}^{i\nu})}{Ca|z_\zeta(\mathrm{e}^{i\nu})|} + \epsilon\alpha^2\cos(2\nu) = C - \epsilon\alpha^2\cos(2\nu), \qquad (5.9)$$

where C is a constant.

To determine C, we invoke the steady-state version of (5.6) and use (5.4) to obtain

$$\frac{\epsilon\alpha^2}{\gamma} = \frac{1}{2\pi i}\int_{|\zeta'|=1}\frac{\mathrm{d}\zeta'}{\zeta'}\left[\frac{\zeta'+\sqrt{\gamma}}{\zeta'-\sqrt{\gamma}}\right]\left\{\frac{\tau(\zeta')}{Ca|z_\zeta(\zeta')|} + \mathrm{Re}\left[\frac{\epsilon\alpha^2}{\zeta'^2}\right]\right\}, \qquad (5.10)$$

where we have used the third equation in (5.6) to eliminate β in favour of α and γ. If we set $\zeta' = \mathrm{e}^{i\theta}$, then $(\zeta'+\sqrt{\gamma})/(\zeta'-\sqrt{\gamma}) = 1 + 2\sum_{n=1}^{\infty}\gamma^{n/2}\mathrm{e}^{-in\theta}$. From (5.9), the integral on the right-hand side of (5.10) can be evaluated, and is $C - \epsilon\alpha^2\gamma$. It follows that

$$C = \epsilon\alpha^2\left(\gamma + \frac{1}{\gamma}\right), \qquad (5.11)$$

and thus, from (5.9), the steady-state tension has the form

$$\tau(\nu) = \epsilon\alpha^2 Ca|z_\zeta(\mathrm{e}^{i\nu})|\left[\left(\gamma + \frac{1}{\gamma}\right) - 2\cos(2\nu)\right]. \qquad (5.12)$$

We note that $\gamma + 1/\gamma \geq 2$, implying that $\tau \geq 0$, so that there are no compressive tensions in the steady state. The second and third equations of (5.6) with (5.12) give the map parameters α, γ, and the tension $\tau(\nu)$ in terms of the map parameter β, the imposed flow parameter ϵ and Ca. Conservation of total reference length (4.20) with choice of the membrane constitutive law then determines the capillary number Ca, given β, ϵ and τ_0.

Figure 6 shows the steady-state solution branch together with representative capsule shapes. The conformal map (5.2), with the second and third equations of (5.6), gives a one-parameter family of shapes parameterized by β, and a critical value $\beta = \beta_c \approx 1.84$ occurs when $z_\zeta = 0$ at $\zeta = \pm 1$. At this point, the map is not conformal and there are two zero-angled cusps at the capsule ends. We note that this specific result also holds in the general time-dependent case. In the steady state, (5.12) implies that the membrane tension is zero there. The critical value $\beta = \beta_c$ is shown by the dotted line in the figure. The steady solution branch intersects this line at $Ca = Ca_c \approx 1.25$, and, for $\beta > \beta_c$, the interface shape given by the map self-intersects so that the solution is unphysical. The implication
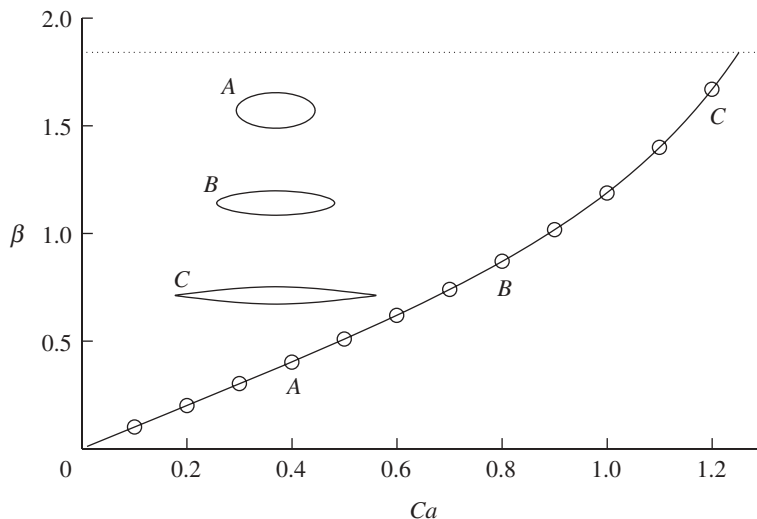
Figure 6. Steady-state values of the map parameter β versus the capillary number Ca for the nonlinear far-field flow (2.9), with $\epsilon = 0.01$ and $\tau_0 = 1$. The solid curve is calculated from the analysis of §5a, and the circles are found from the time-dependent evolution at large t as the interface approaches a steady shape. The dotted line is $\beta = \beta_c$.

is that, for $Ca > Ca_c$, there are no steady capsule shapes, and time-dependent evolution leads to formation of finite-time cusp singularities. Strong numerical evidence for this is provided subsequently.

(b) Time evolution

The initial value problem (5.6)–(5.7) with (4.14) is solved by the same numerical method as described in §4d with the specific far-field flow parameter $\epsilon = 0.01$. When the capillary number Ca is less than the critical value Ca_c, the capsule reaches a steady shape that is in agreement with the analytical solutions presented in §5a (figure 6). An example of the evolution for $Ca > Ca_c$ is shown in figure 7, where $Ca = 5.0$. The interface approaches a shape with zero-angled cusps at $t \simeq 1.1$, and the curvature κ at the capsule ends where the cusps form grows rapidly and without bound. This result is highly suggestive of finite-time singularity formation. The calculation is stopped when the tip curvature is $\kappa = 1.03 \times 10^{13}$. Figure 8 shows evidence for the conformal map parameter β approaching the critical value β_c for cusp formation linearly in time, that is,

$$\beta_c - \beta \sim c(t_c - t), \tag{5.13}$$

where t_c is the singularity time and c is a constant. This will be used in the subsequent analysis.

(i) Similarity solution

The dynamics in a neighbourhood of a cusp singularity, for example near $\nu = 0$ and $t = t_c$, can be shown to be self-similar. We begin by recovering
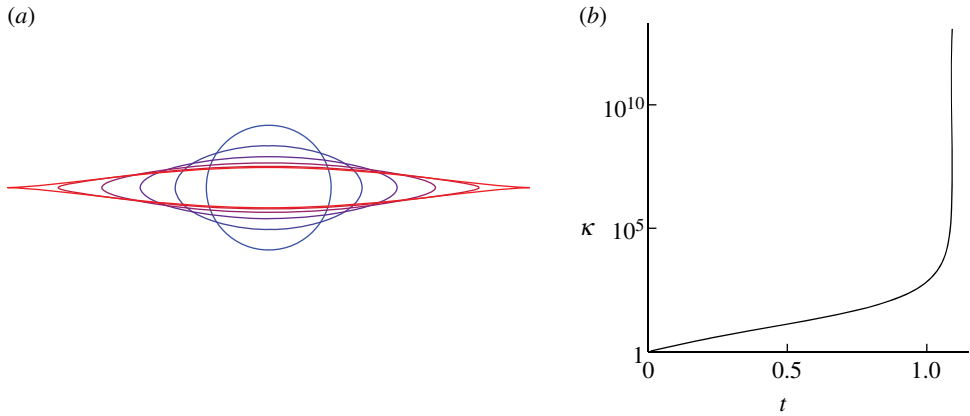
Figure 7. (*a*) Evolution of an initially circular capsule in nonlinear extensional flow with $Ca = 5.0$, $\epsilon = 0.01$ and $\tau_0 = 1$. (*b*) The capsule profiles are shown at intervals of $\Delta t \approx 0.22$. The capsule end curvature κ is plotted versus time t. (Online version in colour.)
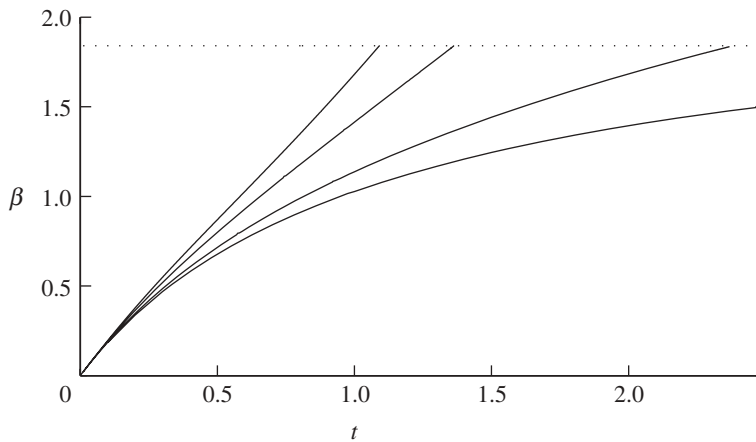

Figure 8. Plot of the map parameter β versus t for $\epsilon = 0.01$, $\tau_0 = 1$ and (from right to left) $Ca = 1.25 (\approx Ca_c), 1.5, 2.5$ and 5.0. For $Ca > Ca_c$, β approaches β_c linearly in time.

from (5.2) the coordinates

$$x(\nu, t) = \frac{(\alpha + \beta - \beta\gamma)\cos(\nu) - \alpha\gamma\cos(3\nu)}{(1 + \gamma^2) - 2\gamma\cos(2\nu)} \tag{5.14}$$

and

$$y(\nu, t) = \frac{(-\alpha + \beta + \beta\gamma)\sin(\nu) + \alpha\gamma\sin(3\nu)}{(1 + \gamma^2) - 2\gamma\cos(2\nu)}. \tag{5.15}$$

Near the endpoint $\nu = 0$,

$$x(\nu, t) = x_0(t) + x_2(t)\nu^2 + O(\nu^4) \tag{5.16}$$

and

$$y(\nu, t) = y_1(t)\nu + y_3(t)\nu^3 + O(\nu^5), \tag{5.17}$$

where

$$x_0(t) = \frac{\alpha + \beta}{1 - \gamma}, \quad x_2(t) = -\frac{\alpha + \beta - 2\alpha\gamma + 6\beta\gamma + 9\alpha\gamma^2 + \beta\gamma^2}{2(1 - \gamma)^3}, \tag{5.18}$$

$$y_1(t) = \frac{-\alpha + \beta + 3\alpha\gamma + \beta\gamma}{(1 - \gamma)^2} \tag{5.19}$$

and $$y_3(t) = \frac{\alpha - \beta - 5\alpha\gamma - 23\beta\gamma - 17\alpha\gamma^2 - 23\beta\gamma^2 - 27\alpha\gamma^3 - \beta\gamma^3}{6(1 - \gamma)^4}. \tag{5.20}$$

We write a local interface representation $x = x(y, t)$ for $y \simeq 0$ by balancing the terms of equation (5.17) and applying Cardano's formula, to give

$$\nu(y, t) = -\frac{1}{3\sqrt[3]{2}}\left[\sqrt[3]{a_1 y + \sqrt{a_1^2 y^2 + a_2}} + \sqrt[3]{a_1 y - \sqrt{a_1^2 y^2 + a_2}}\right], \tag{5.21}$$

where $a_1(t) = -27/y_3$ and $a_2(t) = 12y_1/y_3^3$. At the singularity time, the criterion for the membrane shape not to be smooth is $x_\nu(\nu = 0) = y_\nu(\nu = 0) = 0$, which implies that $y_1(t_c) = 0$. Recall that $z_\zeta(\zeta = 1) = 0$ when $\beta = \beta_c$, and note that (5.19) implies that $y_1(t) \sim c_1(\beta_c - \beta(t))$ for constant c_1 when β is near β_c. Therefore, from (5.13)

$$y_1(t) \sim d(t_c - t) \tag{5.22}$$

at leading order in $t_c - t$, for some constant d. We introduce the similarity variable

$$\xi = \frac{y}{(t_c - t)^{3/2}} \tag{5.23}$$

and deduce from either (5.17) or (5.21) and (5.22) that, for $0 < t_c - t \ll 1$, $\nu(\xi, t) \sim (t_c - t)^{1/2} P(\xi)$, where

$$P(\xi) = -\frac{1}{3\sqrt[3]{2}}\left[\sqrt[3]{\tilde{a}_1\xi + \sqrt{\tilde{a}_1^2\xi^2 + \tilde{a}_2}} + \sqrt[3]{\tilde{a}_1\xi - \sqrt{\tilde{a}_1^2\xi^2 + \tilde{a}_2}}\right] \tag{5.24}$$

and $\tilde{a}_1 = a_1(t_c)$, $\tilde{a}_2 = 12d/y_3^3(t_c)$. Equation (5.16) then implies

$$x - x_0 \sim x_2(t_c)(t_c - t)P^2(\xi) \tag{5.25}$$

for $0 < t_c - t \ll 1$, which is the desired local similarity solution. The curvature at the capsule ends blows up according to

$$\kappa \sim d_1(t_c - t)^{-2}, \tag{5.26}$$
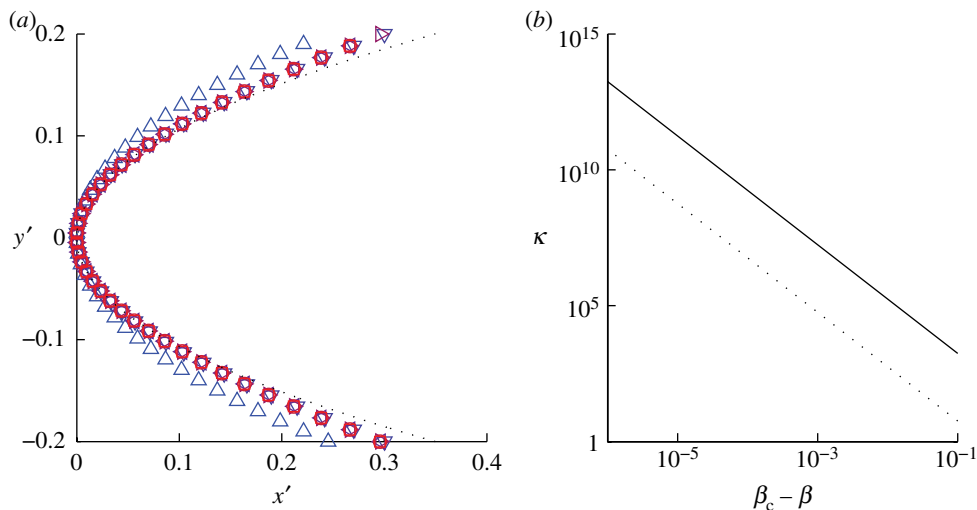
for constant d_1.

Figure 9. Local interface profiles at (*a*) an emerging cusp plotted in terms of the rescaled variables x' and y' for $(\beta_c - \beta) = 1, 10^{-1}, 10^{-2}, \ldots, 10^{-5}$. The curves collapse onto the function $P^2(\xi)$ of (5.24), which is shown as a dotted curve. (*b*) The scaling in equation (5.26) is shown in the log–log plot of tip curvature versus $\beta_c - \beta$. A dotted line of slope -2 is shown for comparison. Data are shown for $\epsilon = 0.01$ and $\tau_0 = 1$. (Online version in colour.)

Numerical verification of the similarity solution is presented in figure 9, which shows the interface shape computed from the time-dependent map near the tip $\nu = 0$ in terms of the rescaled variables

$$x' = \frac{x - x_0}{\beta_c - \beta} \quad \text{and} \quad y' = \frac{y}{(\beta_c - \beta)^{3/2}}. \tag{5.27}$$

This rescaling by $\beta_c - \beta$ is equivalent to rescaling by $t_c - t$ in view of the relation (5.13), but has the advantage that β_c is known analytically whereas t_c is not. Figure 9 shows that interface profiles plotted at times corresponding to a nearly six-decade decrease in $t_c - t$ collapse onto a single curve, which is a representation of the function $P^2(\xi)$. Further, the growth in curvature at the tip closely follows the relation (5.26), as seen in figure 9*b*. Taken together, these results provide strong evidence of self-similar cusp formation during the evolution of a capsule in a nonlinear extensional flow.

The numerical results indicate that, during the time evolution, zeros of z_ζ approach the unit disc in the ζ-plane along the real and imaginary axes, and reach it at $\zeta = \pm 1$ in finite time when cusps form. The distance of the real zeros from the unit disc tends to zero like $t_c - t$. Figure 10 shows the membrane tension at a capsule endpoint and indicates the typical feature that the tension becomes negative some time before the critical instant of cusp formation, t_c. When a transient cusp forms, the membrane tension at the capsule ends appears to tend to zero linearly in time, but from (5.26) it does so more slowly than κ^{-1} so that the capillary stress $\tau\kappa$ tends to infinity. The numerical results indicate that the fluid pressure just outside the cusp remains bounded, while the viscous stress becomes singular.
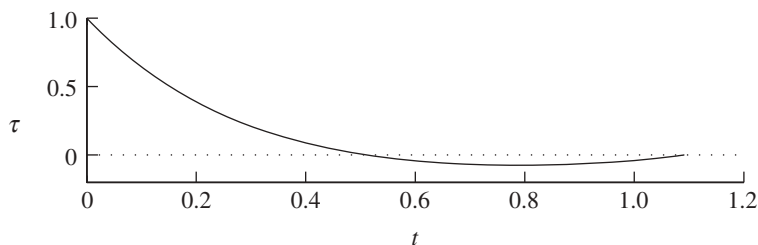
Figure 10. Membrane tension at a capsule endpoint versus time for $Ca = 5.0$, $\epsilon = 0.01$ and $\tau_0 = 1$.

6. Conclusion

We have presented semi-analytical solutions for a two-dimensional elastic capsule enclosing inviscid fluid that evolves in Stokes flow. The solutions are derived by a complex variable formulation that was originally developed to describe the evolution of a bubble in Stokes flow. This paper contains the first application of the method to flow with a deformable elastic surface.

The complex variable technique is based on a conformal map $z(\zeta, t)$ from $|\zeta| < 1$ to the external fluid domain. Apart from a pole at $\zeta = 0$, the map has the form of a truncated polynomial in ζ (4.7) or a rational function of truncated polynomials (5.1) depending on the imposed flow. The evolution is given by the solution of a low-order system of ODEs for the time-dependent coefficients of the map. The imposed flow that stretches the capsule is a strain or shear, and, for much of this study, we choose a simple Hookean constitutive law. The initial shape is a circle with constant membrane tension. We obtain semi-analytical formulae for the capsule shape and membrane tension in the steady state, and we perform efficient, spectrally accurate numerical computations of the time-dependent evolution.

The results show that, when the imposed flow is a linear shear, a steady capsule shape is always attained, regardless of the capillary number. Material points rotate or tank-tread around the steady shape. In a linear strain for Hooke's law or a strain-softening power-law constitutive relation, a steady shape is reached when the capillary number is below a critical value Ca_c. The capsule deformation increases without bound when $Ca > Ca_c$, and the capsule bursts. For a strain-hardening power law, there is no critical capillary number.

We note that, in a simple shear or a nonlinear strain, negative tensions sometimes develop on the membrane during the time evolution, but, by confining the map $z(\zeta, t)$ to the forms (4.7) and (5.1) discussed, the method of solution avoids generation of high wavenumber modes that are associated with ill-posedness and lead to unstable numerics.

We have also considered Antanovskii's nonlinear strain flow to model the far-field velocity in a four-roller mill, and find that steady-state solutions exhibit an increasing tip curvature with increasing capillary number. There is a critical capillary number Ca_c, at which the steady capsule is cusp-shaped, and, for $Ca > Ca_c$, there are no physically realizable steady shapes. The time-dependent evolution leads to self-similar cusp formation at a finite critical time t_c. A local similarity solution is found analytically (see equations (5.25) and (5.26)), which is confirmed by numerical examples. The cusped solution provides a test for other numerical methods and we expect it to be useful in their validation.

In addition to the limitation to two dimensions, which omits the effect of out-of-plane membrane tension, several physical effects are left out of the present study. We consider an inviscid interior fluid and no membrane bending stiffness. Indeed, the exact truncation of the conformal map, which is central to this study, is no longer valid when bending stiffness is included.

References

Antanovskii, L. K. 1996 Formation of a pointed drop in Taylor's four-roller mill. *J. Fluid Mech.* **327**, 325–341. (doi:10.1017/S0022112096008567)

Barthès-Biesel, D. 1980 Motion of a spherical microcapsule freely suspended in a linear shear flow. *J. Fluid Mech.* **100**, 831–853. (doi:10.1017/S0022112080001449)

Barthès-Biesel, D. 1991 Role of interfacial properties on the motion and deformation of capsules in shear flow. *Physica A* **172**, 103–124. (doi:10.1016/0378-4371(91)90314-3)

Barthès-Biesel, D. 2011 Modeling the motion of capsules in flow. *Curr. Opin. Colloid Interface* **16**, 3–12. (doi:10.1016/j.cocis.2010.07.001)

Barthès-Biesel, D., Diaz, A. & Dhenin, E. 2002 Effect of constitutive laws for two-dimensional membranes on flow-induced capsule deformation. *J. Fluid Mech.* **460**, 211–222. (doi:10.1017/S0022112002008352)

Bazant, M. Z. & Crowdy, D. 2005 Conformal mapping methods for interfacial dynamics. *Handb. Mater. Model.* **1**, 1417–1451.

Beale, J. T. & Strain, J. 2008 Locally corrected semi-Lagrangian methods for Stokes flow with moving elastic interfaces. *J. Comput. Phys.* **227**, 3896–3920. (doi:10.1016/j.jcp.2007.11.047)

Blomley, M. J. K., Cooke, J. C., Unger, E. C., Monaghan, M. J. & Cosgrove, D. O. 2001 Microbubble contrast agents: a new era in ultrasound. *Br. Med. J.* **322**, 1222–1225. (doi:10.1136/bmj.322.7296.1222)

Chang, K. S. & Olbricht, W. L. 1993 Experimental studies of the deformation and breakup of a synthetic capsule in steady and unsteady simple shear flow. *J. Fluid Mech.* **250**, 609–633. (doi:10.1017/S0022112093001582)

Crowdy, D. & Siegel, M. 2005 Exact solutions for the evolution of a bubble in Stokes flow: a Cauchy transform approach. *SIAM J. Appl. Math.* **65**, 941–963. (doi:10.1137/S0036139903430847)

Dodson, W. & Dimitrakopoulos, P. 2008 Spindles, cusps, and bifurcation for capsules in Stokes flow. *Phys. Rev. Lett.* **101**, 2–5. (doi:10.1103/PhysRevLett.101.208102)

Dodson, W. & Dimitrakopoulos, P. 2009 Dynamics of strain-hardening and strain-softening capsules in strong planar extensional flows via an interfacial spectral boundary element algorithm for elastic membranes. *J. Fluid Mech.* **641**, 263–296. (doi:10.1017/S0022112009991662)

Eggers, J., Lister, J. R. & Stone, H. A. 1999 Coalescence of liquid drops. *J. Fluid Mech.* **401**, 293–310. (doi:10.1017/S002211209900662X)

Jeffery, G. B. 1922 The motion of ellipsoidal particles immersed in a viscous fluid. *Proc. R. Soc. Lond. A* **102**, 161–179. (doi:10.1098/rspa.1922.0078)

Krasny, R. 1986 A study of singularity formation in a vortex sheet by the point-vortex approximation. *J. Fluid Mech.* **167**, 65–93. (doi:10.1017/S0022112086002732)

Kropinski, M. C. A. 2001 An efficient numerical method for studying interfacial motion in two-dimensional creeping flows. *J. Comput. Phys.* **171**, 479–508. (doi:10.1006/jcph.2001.6787)

Lac, E., Barthès-Biesel, D., Pelekasis, N. A. & Tsamopoulos, J. 2004 Spherical capsules in three-dimensional unbounded Stokes flows: effect of the membrane constitutive law and onset of buckling. *J. Fluid Mech.* **516**, 303–334. (doi:10.1017/S002211200400062X)

Langlois, W. E. 1964 *Slow viscous flow.* New York, NY: Macmillan.

Mikhlin, S. G. 1957 *Integral equations.* New York, NY: Pergamon Press.

Navot, Y. 1998 Elastic membranes in viscous shear flow. *Phys. Fluids* **10**, 1819–1833. (doi:10.1063/1.869702)

Pozrikidis, C. 1992 *Boundary integral and singularity methods for linearized viscous flow.* Cambridge, UK: Cambridge University Press.

Pozrikidis, C. 1995 Finite deformation of liquid capsules enclosed by elastic membranes in simple shear flow. *J. Fluid Mech.* **297**, 123–152. (doi:10.1017/S002211209500303X)

Pozrikidis, C. 2003 *Modeling and simulation of capsules and biological cells.* Boca Raton, FL: CRC Press.

Ramanujan, S. & Pozrikidis, C. 1998 Deformation of liquid capsules enclosed by elastic membranes in simple shear flow: large deformations and the effect of fluid viscosities. *J. Fluid Mech.* **361**, 117–143. (doi:10.1017/S0022112098008714)

Richardson, S. 1968 Two-dimensional bubbles in slow viscous flows. *J. Fluid Mech.* **33**, 476–493. (doi:10.1017/S0022112068001461)

Richardson, S. 1997 Two-dimensional Stokes flows with time-dependent free boundaries driven by surface tension. *Euro. J. Appl. Math.* **8**, 311–329.

Siegel, M. 1999 Influence of surfactant on rounded and pointed bubbles in two-dimensional Stokes flow. *SIAM J. Appl. Math.* **59**, 1998–2027. (doi:10.1137/S0036139997327435)

Siegel, M. 2000 Cusp formation for time-evolving bubbles in two-dimensional Stokes flow. *J. Fluid Mech.* **412**, 227–257. (doi:10.1017/S002211200000834X)

Stoer, J. & Bulirsch, R. 2002 *Introduction to numerical analysis*, 3rd edn. Berlin, Germany: Springer.

Tanveer, S. & Vasconcelos, G. L. 1995 Time-evolving bubbles in two-dimensional Stokes flow. *J. Fluid Mech.* **301**, 325–344. (doi:10.1017/S0022112095003910)

Taylor, G. I. 1934 The formation of emulsions in definable fields of flow. *Proc. R. Soc. Lond. A* **146**, 501–523. (doi:10.1098/rspa.1934.0169)

Veerapaneni, S. K., Gueyffier, D., Zorin, D. & Biros, G. 2009 A boundary integral method for simulating the dynamics of inextensible vesicles suspended in a viscous fluid in 2D. *J. Comput. Phys.* **228**, 2334–2353. (doi:10.1016/j.jcp.2008.11.036)

Walter, J., Salsac, A. V., Barthès-Biesel, D. & Le Tallec, P. 2010 Coupling of finite element and boundary integral methods for a capsule in a Stokes flow. *Int. J. Numer. Method Eng.* **83**, 829–850. (doi:10.1002/nme.2859)